

Assessment of blockage effects on the wake characteristics and power of wind turbines



H. Sarlak ^{a,*}, T. Nishino ^b, L.A. Martínez-Tossas ^c, C. Meneveau ^c, J.N. Sørensen ^a

^a Fluid Mechanics Section, Department of Wind Energy, Technical University of Denmark, 2800, Lyngby, Denmark

^b Centre for Offshore Renewable Energy Engineering, Cranfield University, Cranfield, Bedfordshire, MK43 0AL, UK

^c Department of Mechanical Engineering, Johns Hopkins University, Baltimore, MD, 21218, USA

ARTICLE INFO

Article history:

Received 1 July 2015

Received in revised form

4 December 2015

Accepted 31 January 2016

Available online xxxx

Keywords:

Large eddy simulation

Wind turbine wake

Power characteristics

Actuator line

Blockage effect

Tip speed ratio

Tip correction

ABSTRACT

Large Eddy Simulations (LES) are performed in order to study the wake and power characteristics of a horizontal-axis wind turbine in a wind tunnel. Using an actuator line technique, the effect of wind tunnel blockage ratio (defined as the ratio of the rotor swept area to the tunnel cross-sectional area) is investigated for a wide range of tip speed ratios from 1 to 12, and for four blockage ratios (0.2, 0.09, 0.05 and 0.02). The results demonstrate how the blockage effect increases with the tip speed ratio. When the tip speed ratio is close to or above the optimal design value, blockage ratios of larger than 0.05 affect both tangential and normal forces on the blades and therefore on the power and thrust coefficients. At the highest blockage ratio of 0.2, the mean velocity of the wake is also affected significantly, although the effect on the wake mixing rate is less pronounced. Further, the effect of the Reynolds number on the wake development is illustrated and the impact of numerics and subgrid-scale models are investigated by comparing two different LES codes. Finally, the importance of tip loss correction in actuator-line modeling of wind turbines is illustrated using comparative computations.

© 2016 Elsevier Ltd. All rights reserved.

1. Introduction

When performing actuator-line simulations to study the characteristics of wind turbine wakes, it is common to consider a large computational domain to minimize the effect of the boundary conditions representing the lateral walls. This contradicts the real turbine wake measurements in a wind tunnel, where the effect of flow confinement, or blockage, is often important. In the present paper, blockage ratio is defined as the ratio of the rotor swept area to the tunnel cross-sectional area. The issue of blockage is also of high importance when studying a lateral array of wind turbines in an open atmosphere, where the flow passage around each turbine is confined by the neighboring turbines [20]. It is therefore useful to systematically assess the effect of blockage on the wake characteristics as well as the operation and efficiency of wind turbines.

The effect of blockage has been a subject of a number of aerodynamic studies in the past. For example [18], investigated the wall interference problem associated with two-dimensional wind tunnel testing at subsonic and transonic speeds. For three-dimensional

delta-wing applications, it has been shown using Euler and Reynolds-averaged Navier–Stokes (RANS) simulations, that a major effect of sidewall proximity is to promote vortex breakdown [2,8] studied the wall effects on two tandem cylinders at low Reynolds number. Also, Patil and Tiwari [23] investigated the effects of blockage ratio on wake transition for flow past a square cylinder using 2D simulations and showed that the wall confinement has an impact on the value of critical Reynolds number above which planar vortex shedding occurs.

With regard to turbine applications, the blockage effect was first studied experimentally by Glauert on constantly loaded rotor discs (representing propellers) [6]. Glauert's correction is derived from the momentum balance in terms of the velocity adjustment in the tunnel. The blockage correction has since been investigated theoretically, numerically, and experimentally in numerous studies [1,5,27,43]. Medici et al. [14] performed PIV measurements on a two-bladed and a three-bladed wind turbine model to investigate the blockage effects in the upstream region of the rotor and proved that the flow can be affected as far as 3 rotor diameters upstream the rotor plane, with a change in the turbine operation. Recently, Nishino and Willden [21] studied the effects of channel geometry on the performance of tidal turbines, using incompressible RANS

* Corresponding author.

E-mail address: hsar@dtu.dk (H. Sarlak).

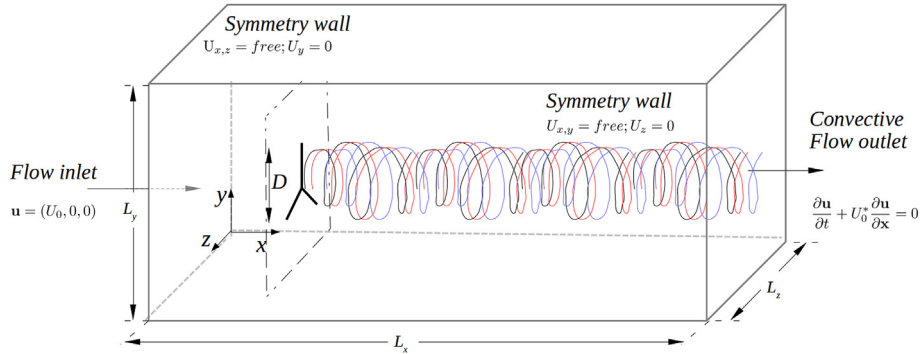


Fig. 1. A sketch of the computational domain.

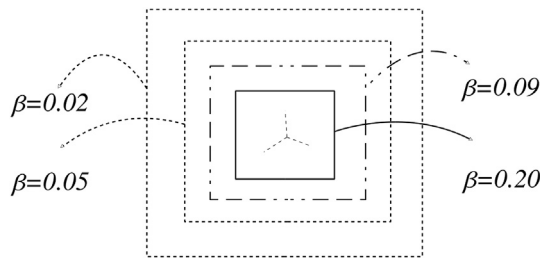


Fig. 2. Schematic diagram of the different blockage ratios considered.

simulations with an actuator disc representation of turbines and proposed an approach to account for the effect of turbulence generated by the turbines. McTavish et al. [13] examined the effects of blockage on the initial wake expansion behind a wind turbine using dye visualization to characterize the propagation of tip vortices from different rotors in a closed wind tunnel.

While many of the previous studies on the tunnel blockage effect have dealt with 2D flows and/or RANS simulations, being

valuable when simple geometries and/or time-averaged values are of interest (e.g. power, thrust and wake deficit), these methods are unable to provide detailed information of the flow such as turbulent flow structures and tip/root vortices. For the latter purpose, Large Eddy Simulation (LES) technique has in recent years become a common tool due to the advances in computational power. In the LES approach, the flow field is decomposed into a filtered and a fluctuating part. The energy containing large flow structures are directly simulated whereas the smaller scales — which are responsible for dissipation of the kinetic energy — are modeled by means of subgrid-scale models that enable one to express the effects of smaller scale as function of the resolved flow field. This approach reduces computational requirements drastically compared to the Direct Numerical Simulation (DNS) of the Navier–Stokes equations, especially in non-wall bounded flows (see Refs. [15,24]).

Several studies using LES have been performed in recent years in order to understand the aerodynamic nature of turbine operation. Special attentions have been paid to the structure of wind turbine wakes [17,32,35,40,41,42], interactions of wind turbine wakes with the atmospheric boundary layer [4,9,33,34], and detailed numerical

Table 1

List of studied configurations. The domain length is nondimensionalised with rotor radius, R. Some selected cases were run with a pseudo-spectral code (the JHU code, see section 3.3), for cases $\beta=0.20$ and 0.05 , for laminar inflow and without molecular viscosity.

β	Re	Domain size $R^{-1} \times 25 \times 4 \times 4$	λ	Mesh points	Tip correction	Free stream
0.20	1000	896 × 128 × 128	3	25 × 4 × 4	Shen	Laminar
	1000	896 × 128 × 128	6	25 × 4 × 4	Shen	Laminar
	100,000	896 × 128 × 128	3	Shen	Laminar	
	100,000	25 × 4 × 4	6	896 × 128 × 128	Shen	Laminar
	100,000	25 × 4 × 4	12	896 × 128 × 128	Shen	Laminar
	100,000	25 × 4 × 4	3	896 × 128 × 128	Shen	Turbulent
	100,000	25 × 4 × 4	6	896 × 128 × 128	Shen	Turbulent
	100,000	25 × 4 × 4	12	896 × 128 × 128	Shen	Turbulent
	100,000	25 × 4 × 4	3	896 × 128 × 128	N/A	Laminar
	100,000	25 × 4 × 4	6	896 × 128 × 128	N/A	Laminar
	100,000	25 × 4 × 4	12	896 × 128 × 128	N/A	Laminar
	100,000	25 × 4 × 4	3	896 × 128 × 128	N/A	Laminar
	100,000	25 × 4 × 4	6	896 × 128 × 128	N/A	Turbulent
	100,000	25 × 4 × 4	12	896 × 128 × 128	N/A	Turbulent
	1,000,000	25 × 4 × 4	3	896 × 128 × 128	Shen	Laminar
	1,000,000	25 × 4 × 4	6	896 × 128 × 128	Shen	Laminar
0.09	100,000	26.8 × 6 × 6	3	960 × 160 × 160	Shen	Laminar
	100,000	26.8 × 6 × 6	6	960 × 160 × 160	Shen	Laminar
	100,000	26.8 × 6 × 6	12	960 × 160 × 160	Shen	Laminar
	100,000	26.8 × 6 × 6	3	960 × 160 × 160	Shen	Turbulent
	100,000	26.8 × 6 × 6	6	960 × 160 × 160	Shen	Turbulent
	100,000	26.8 × 6 × 6	12	960 × 160 × 160	Shen	Turbulent
0.05	100,000	23.2 × 8 × 8	6	832 × 208 × 208	Shen	Laminar
	100,000	23.2 × 8 × 8	6	832 × 208 × 208	Shen	Turbulent
0.02	100,000	28.6 × 12 × 12	6	1024 × 256 × 256	Shen	Laminar
	100,000	28.6 × 12 × 12	6	1024 × 256 × 256	Shen	Turbulent

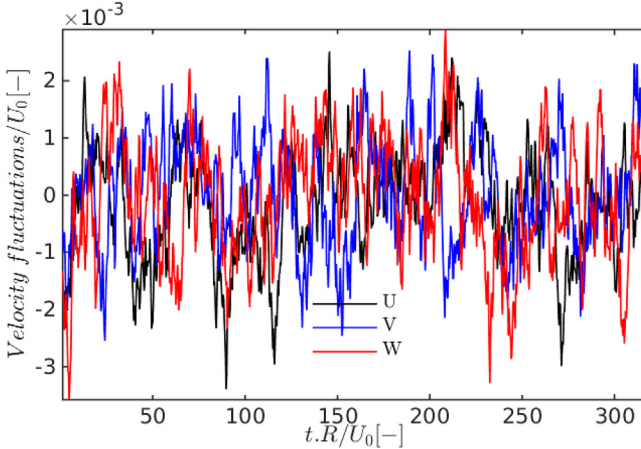


Fig. 3. Velocity fluctuations, introduced at the inlet for the turbulent free stream cases.

and turbulence modeling techniques [30,31,45]. To the extent of authors' knowledge however, the effects of wall confinement on the structures of tip/root vortices in the near wake and turbulent structures in the far wake have not been investigated in detail.

2. Governing equations

For the computations, the three-dimensional incompressible Navier–Stokes equations in primitive variables are solved numerically using the LES technique,

$$\frac{\partial \mathbf{v}}{\partial t} + \mathbf{v} \cdot \nabla \mathbf{v} = -\frac{\nabla p}{\rho} + \nabla \cdot \left[(\nu + \nu_{sgs}) (\nabla \mathbf{v} + \nabla \mathbf{v}^T) \right] + \frac{\mathbf{f}}{\rho}, \quad (1)$$

where \mathbf{v} represents the filtered velocity vector, p is the modified pressure, ρ and ν are the fluid density and molecular viscosity, respectively, ν_{sgs} is the eddy viscosity to be specified by the SGS model (see section 3.3), and \mathbf{f} is the external body force acting on the flow to represent wind turbine blades. For the simulation of wind turbines, the Actuator Line (AL) technique [39] is used, where the body forces representing blades are obtained according to,

$$\mathbf{f} = (L, D) = 0.5\rho V_{rel}^2 c (C_L \mathbf{e}_L + C_D \mathbf{e}_D), \quad (2)$$

Here V_{rel} is the relative velocity, C_L and C_D are lift and drag coefficients, \mathbf{e}_L and \mathbf{e}_D are unit vectors showing the direction of the (local) lift (L) and drag (D) forces and c is the airfoil section chord length. These forces are commonly smeared out by a Gaussian regularization function which is applied to the flow field through the following convolution of the computed load \mathbf{f} and the regularization kernel η_ϵ ,

$$\mathbf{f}_\epsilon = \mathbf{f} \otimes \eta \quad \eta_\epsilon(d) = \epsilon^{-3} \pi^{-3/2} \exp \left[-\left(\frac{d}{\epsilon} \right)^2 \right], \quad (3)$$

where d is the distance between cell centered grid points and points of the actuator line. Here, ϵ is the smearing parameter that serves to adjust the distribution width of the regularized load. The smeared forces are then sampled into the CFD mesh points.

3. Numerical modeling

3.1. Problem set up

Numerical simulations are performed on a scaled wind turbine

used in the blind test experiments at the Norwegian University of Science and Technology (NTNU). The blades consist of the 14% thick NREL S826 airfoil and are assumed to be stiff. The model has a rotor diameter of $D = 0.894$ m and is designed to operate at 10 m/s with a tip speed ratio of $TSR = 6$ [10]. The rotor is subject to uniform laminar and turbulent free stream velocities of $U_0 = 1$. Aerodynamics of the airfoil have been obtained through a series of wind tunnel measurements at the Technical University of Denmark [29].

Computations have been performed in a rectangular computational domain as shown in Fig. 1. To represent the turbine, the actuator line technique proposed by Ref. [39] is used. For all cases, a uniform grid with constant spacing of $\frac{\Delta x}{R} = 0.028$ in the rotor region is used. In addition, the grid spacing in the rotor plane is also kept constant and each actuator line is represented by 35 points along the blade. Parameters of the actuator line are chosen according to Sarlak et al. [30,31]: a force smearing parameter of $\epsilon=2.5$ is chosen. We test four different blockage ratios in this study, as illustrated in Fig. 2.

The studied cases are presented in Table 1. Computations are carried out at three different Reynolds numbers from 1000 to 1,000,000, for a low tip speed ratio of $\lambda=3$, a design tip speed ratio of $\lambda=6$, and a highly loaded case corresponding to $\lambda=12$. In addition to the above cases, several shorter computations with tip speed ratios between 1 and 12 are performed in order to examine the rotor performance such as power and thrust coefficients. The size of the computational domain size and the grid resolutions are also summarized in the table. Unless specified, results presented in this paper are those with the tip correction proposed by Refs. [37,38].

The grid is uniform in the streamwise direction and in the rotor plane, and stretched in the lateral and vertical directions out towards the boundaries. The domain sizes in the streamwise direction are chosen such that the spacing between cells are the same in all cases. The location of rotor is also fixed at $x/R=8$ from the inlet section.

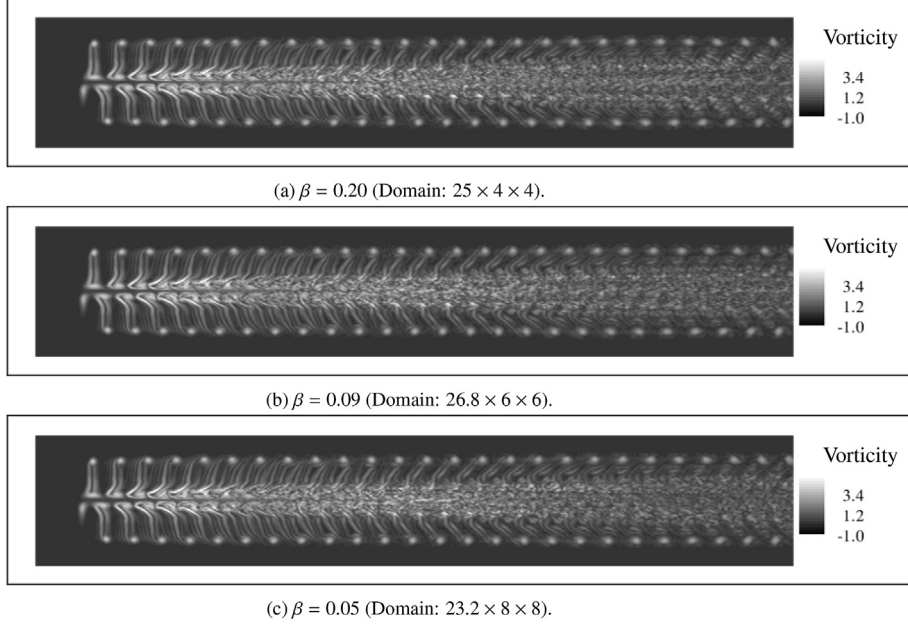
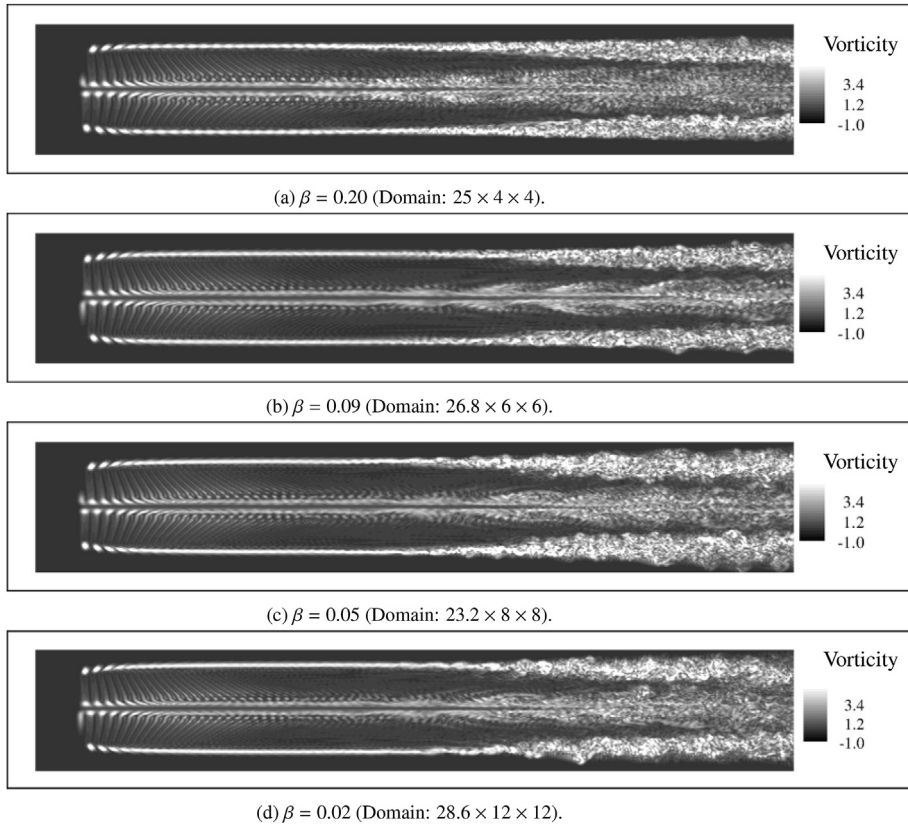
To generate an unsteady turbulent flow at the inlet, an isotropic turbulent field is first generated using the method of Mann [11] and implemented into the computational domain [30,31]: using the Taylor frozen turbulence hypothesis, the 2D planes of turbulent motion are extracted alongside the turbulence box and inserted at three rotor radii upstream of the turbine to produce the desired unsteady flow. For the turbulent inflow cases, a constant inflow velocity with a low free-stream resolved turbulence of 0.24% intensity is introduced at the inlet. Fig. 3 shows the velocity fluctuations introduced at the inlet for the turbulent free stream cases.

3.2. Boundary conditions

As described in Fig. 1, a uniform velocity (with and without perturbations) is introduced at the inlet. Convective outflow boundary condition is used at the outlet, in order to prevent reflections or significant disturbances back into the flow field. In the figure, $\mathbf{u}=(U_x, U_y, U_z)$ is the flow field and U_0^* is the mean convective flow—a universal velocity scale that maintains the overall mass conservation—which can be chosen as the inlet velocity since we are solving an incompressible flow ($U_0^* = U_0$). At the lateral and vertical walls, symmetry boundary conditions are applied and grid clustering due to the boundary layer effects is avoided. The growth of the boundary layer is taken into account by having a constant tunnel height rather than including the slope of the wind tunnel (the experiments were performed in a wind tunnel with a slightly expanding test section).

3.3. Numerical methods

Two different CFD codes are used for the computations in order

**Fig. 4.** Vorticity contours in laminar inflow at $\lambda = 3$ for different domain sizes.**Fig. 5.** Vorticity contours in laminar inflow at $\lambda = 6$ for different domain sizes.

to examine the robustness of the results. The first code, called *DTU code* hereafter, uses a finite volume methodology on collocated grid arrangement to solve the governing equations. Finite volume methodology is used due to the conservation properties [22]. In order to minimize the numerical dissipation, a fourth-order central

differencing is used for the convective terms. This is common practice in LES, to avoid numerical errors of the same order of magnitude as the effect of subgrid scale stresses. Experience shows, however, that employing pure central schemes pose numerical instability (wiggles) in the flow field. To cope with this problem,

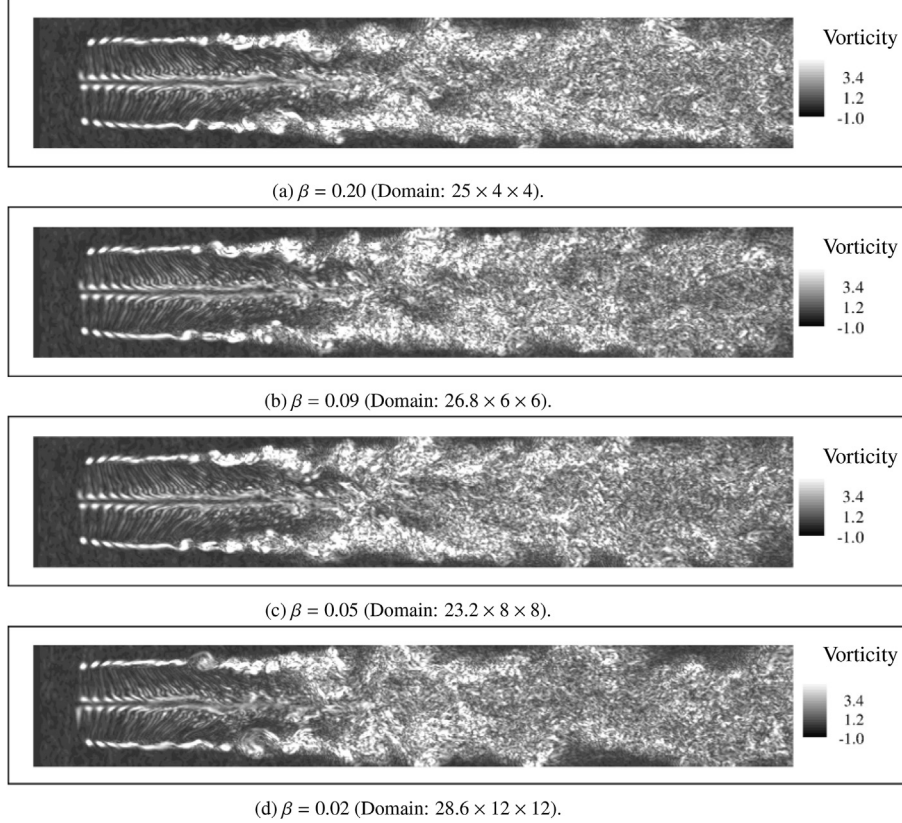


Fig. 6. Vorticity contours in turbulent inflow at $\lambda = 6$ for different domain sizes.

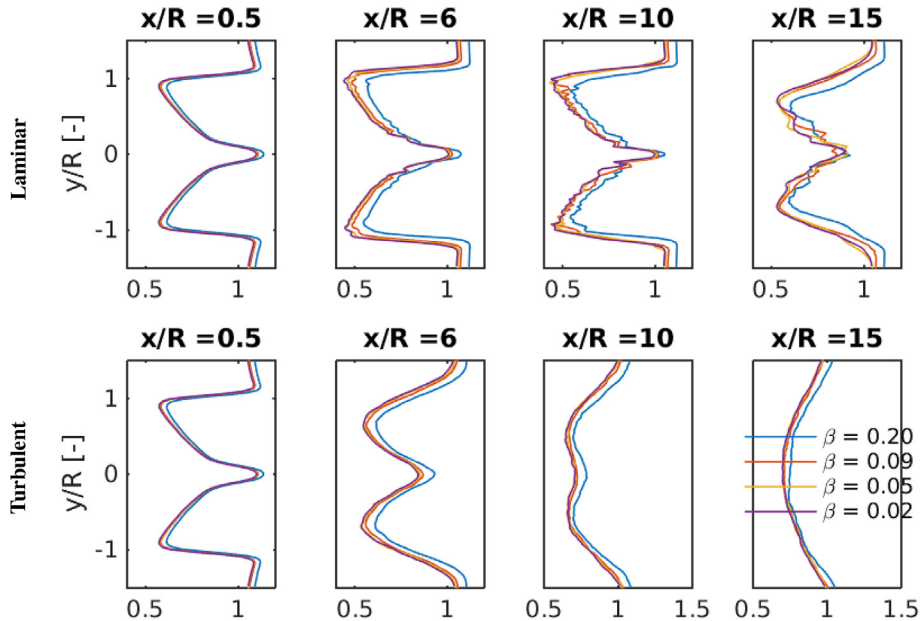


Fig. 7. Time averaged streamwise velocity profiles downstream of the turbine, using laminar (up) and turbulent (down) free stream conditions with $\lambda=6$ and different blockage ratios.

third-order quadratic upwind interpolation is blended (10%) with the fourth-order central schemes (90%) to discretize the convective terms.

Time is discretized using a second order backward Euler scheme and the solution is marched in time using inner time stepping where the number of each pseudo time step can be either specified

or remain as a function of the residuals. The variables are collocated in cell-centers, which may result in pressure oscillations. In order to avoid such non-physical oscillations, the pressure–velocity coupling method proposed by Ref. [26] is used to account for advective velocities. The pressure correction equation is handled using the PISO algorithm [7].

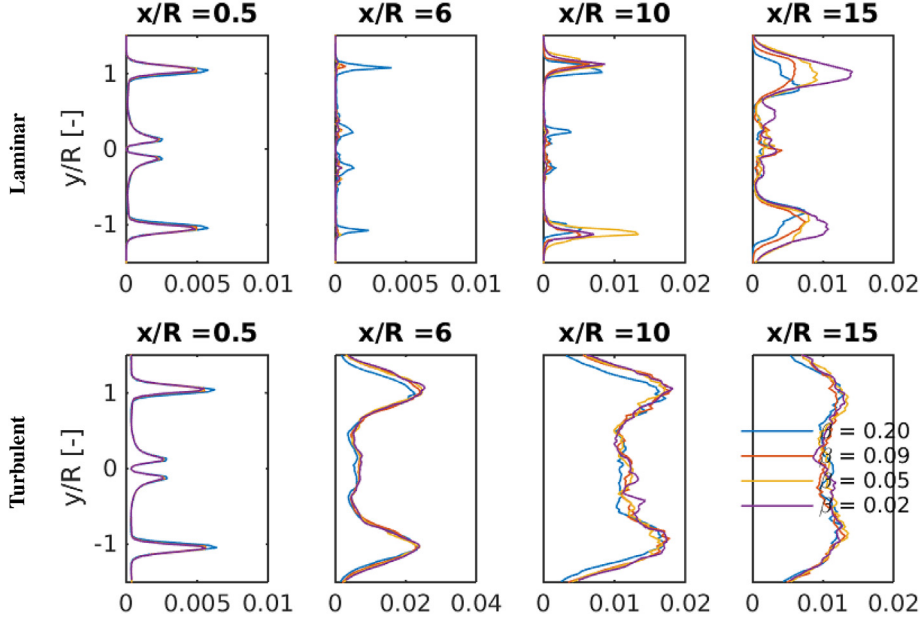


Fig. 8. Profiles of the resolved turbulent kinetic energy downstream of the turbine, using laminar (up) and turbulent (down) free stream conditions with $\lambda=6$ and different blockage ratios.

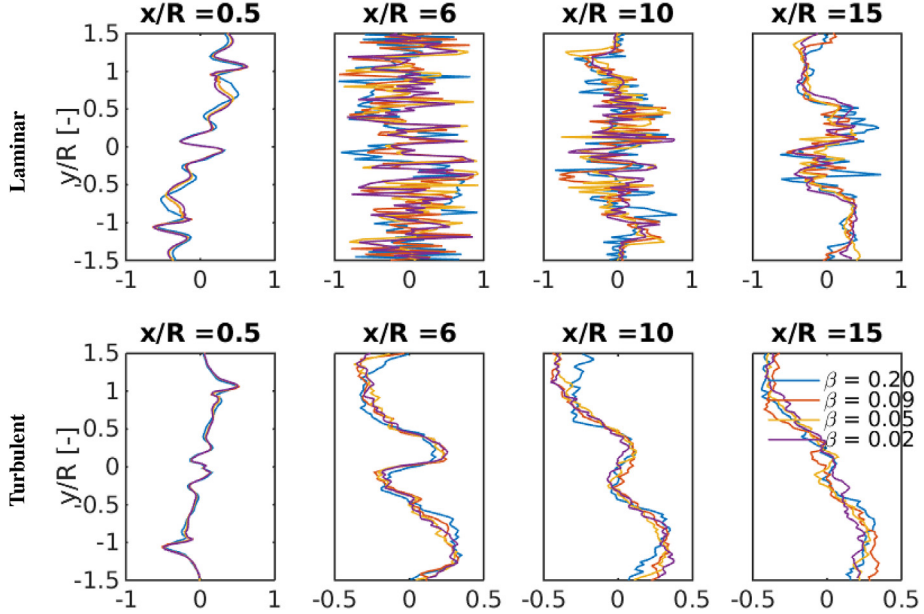


Fig. 9. Profiles of the normalized Reynolds stress downstream of the turbine at $\lambda=6$ with laminar (up) and turbulent (down) free stream conditions.

In the DTU code, we consider an eddy-viscosity closure in which time-scales are parameterized using the resolved rotation rate (vorticity) for the SGS parametrization. This model is based on the approach proposed by Refs. [28,44] to compute the eddy viscosity, ν_{sgs} , namely:

$$\nu_{sgs} = c_{MO} \Delta^{1.5} q_c^{0.25} |\bar{\Omega}|^{0.5} \quad (4)$$

where $c_{MO}=0.02$ is a constant, $\Delta=(\delta x \times \delta y \times \delta z)^{1/3}$ is the grid filter width and $\bar{\Omega}$ is the vorticity vector. The kinetic energy-scale q_c is defined and computed according to $q_c = (\bar{u}_i - u_i)(\bar{u}_i - u_i)$, where \bar{u}_i represents the velocity, explicitly filtered at scale $\tilde{\Delta}$, where $\tilde{\Delta}/\Delta$, and

can be evaluated using a 3D volume averaging using stencils of size 27 with trapezoidal weights that mimic a box filter [29].

The DTU code has been extensively validated against available experimental data [16]. For a recent, detailed comparison of LES data against available wind farm measurements see Ref. [19]. The numerical set up used in the current study has been specifically subject to code validation against rotor measurements (see Refs. [30,31,35]), where it was shown, by investigating various grid sizes, free stream turbulence intensities, SGS models, and tip speed ratios, that the code is capable of predicting the dynamics of wind turbine wakes with high accuracy. Numerical settings used in this paper are based on the previous findings and therefore, to keep the length of this paper short, and since the main aim of the current

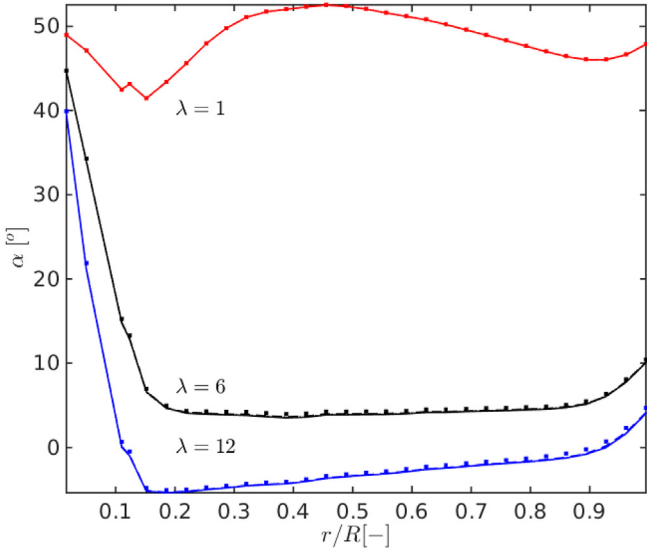


Fig. 10. Effect of the tip speed ratio and tunnel confinement on the computed local angle of attack across the blade in laminar free stream. Various markers indicate different blockage ratios: [...] $\beta=0.2$, [---] $\beta=0.09$, [.-.] $\beta=0.05$, [—] $\beta=0.02$.

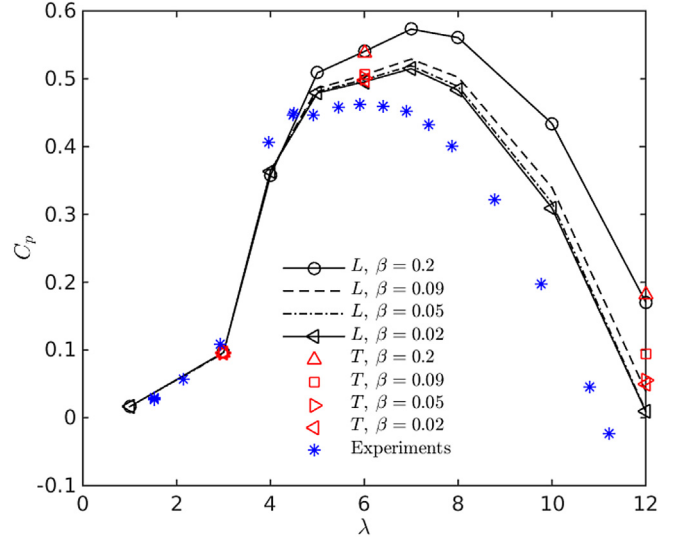


Fig. 13. Effect of the blockage ratio on the power coefficient of turbine subject to different values of tip speed ratio (L: laminar free stream; T: turbulent free stream).

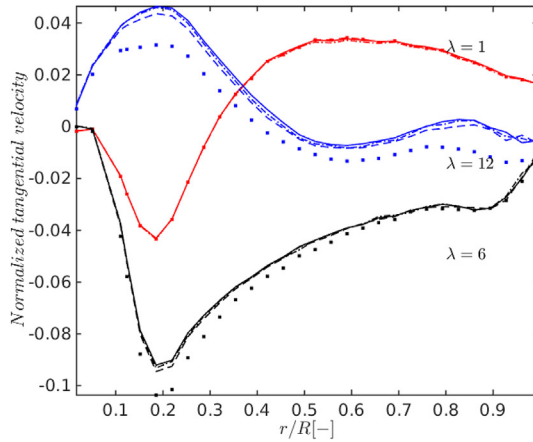


Fig. 11. Effect of the tip speed ratio and tunnel confinement on the computed tangential (left) and normal (right) velocities on the blade in laminar free stream. Various markers indicate different blockage ratios: [...] $\beta=0.2$, [---] $\beta=0.09$, [.-.] $\beta=0.05$, [—] $\beta=0.02$.

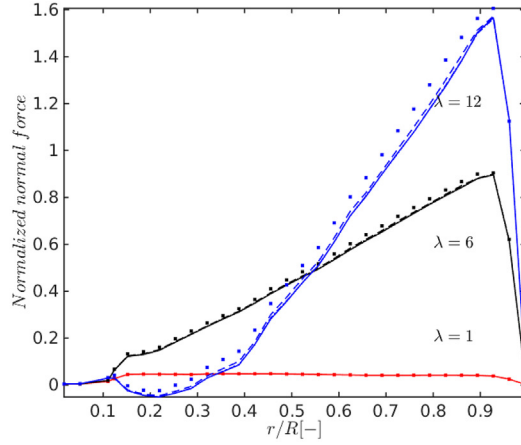
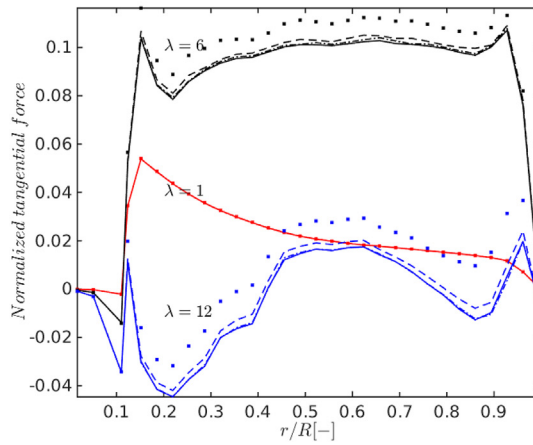
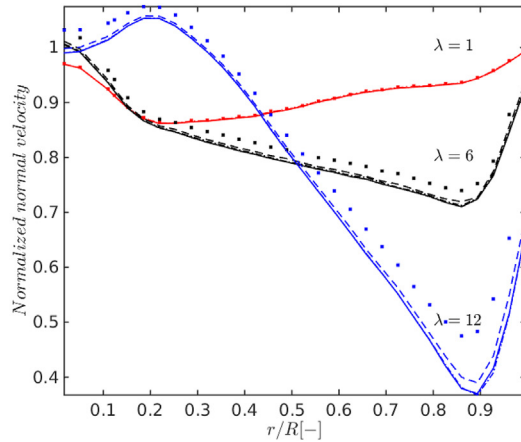


Fig. 12. Effect of the tip speed ratio and tunnel confinement on the computed tangential (left) and normal (right) forces on the blade in laminar free stream. Various markers indicate different blockage ratios: [...] $\beta=0.2$, [---] $\beta=0.09$, [.-.] $\beta=0.05$, [—] $\beta=0.02$.

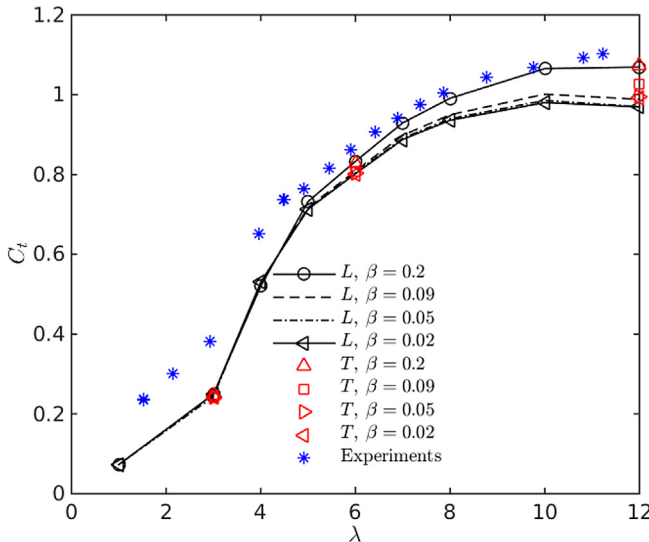


Fig. 14. Effect of the blockage ratio on the thrust coefficient of turbine subject to different values of tip speed ratio (L: laminar free stream; T: turbulent free stream).

research is to investigate the effects of confinement in the wake dynamics, further code validations are not shown in this paper.

Simulations are run for two Non-dimensional Time Units (NTU)¹ first, which is long enough for the flow to reach a statistically stationary state. The subsequent averaging takes place for about 3 NTUs to ensure that the high order statistical moments are converged. The mean streamwise velocity and streamwise turbulence intensity profiles are compared with the measurements at four locations downstream of the turbine.

The second CFD code, the in-house code developed at the Johns Hopkins University and referred to as the *JHU code* hereafter, is a pseudo-spectral CFD solver. Besides the difference in the discretization methods, the JHU code uses the Lagrangian scale-dependent dynamic Smagorinsky model, in which the eddy viscosity is given by $\nu_{sgs} = (c_s \Delta)^2 S$ where S is the strain rate tensor, and c_s is computed dynamically using Lagrangian averaging [3,4]. Time advancement is performed using a second order Adams-Bashforth scheme. The streamwise (x) and lateral (y) directions are spectral while the vertical (z) direction uses second-order centered finite differencing [3,4]. Comparisons with results from this code can be used to ascertain whether numerical discretization, subgrid-scale model or Reynolds number (at high Reynolds numbers) have any appreciable effects on the blockage ratio trends to be studied in this paper.

The domain size and grid resolution is the same and 15% of the domain in the x direction is added as a fringe region to force the velocity to uniform inflow. An actuator line model is implemented in this code [12] and a Gaussian filtering of the force is used, with a smearing parameter of $\epsilon^*=2.5$. The actuator line implementation in the JHU code does not include a tip-loss correction. Two cases were simulated at $\beta=0.2$ and $\beta=0.05$, using a laminar inflow and neglecting the effect of molecular viscosity.

4. Results and discussion

4.1. Blockage effects on the wake

It is known that blockage has an impact on the power and thrust coefficients. In this paper, due to the access to high-resolution numerical data, we also investigate the effects of blockage on vortical wake structures of the turbine. Figs. 4 and 5 investigate such effects in the laminar free stream case. Shown in Fig. 4 are the vorticity fields obtained at $\lambda=3$ with three different tunnel sections, where no noticeable difference can be observed from the qualitative figures. At a higher tip speed ratio of $\lambda=6$, however, as shown in Fig. 5, the impact of confinement on the vortices is slightly more pronounced.

Fig. 6 shows the vorticity contours for the same tip speed ratio ($\lambda=6$) in turbulent free stream. As mentioned earlier, a resolved turbulent inflow of 0.24% intensity is used for the turbulent cases. As can be noticed, introduction of turbulence, even with small magnitude, results in an earlier breakdown of the tip and root vortices. However, again it is difficult to recognize visually the effect of blockage in these qualitative figures.

Figs. 7 and 8 show the profiles of time averaged streamwise velocity \bar{u} and resolved turbulent kinetic energy $k = \frac{1}{2}(\bar{u}'\bar{u}' + \bar{v}'\bar{v}' + \bar{w}'\bar{w}')$, respectively, at four sections downstream of the rotor plane² that is, at the vicinity of the rotor ($x/R=0.5$), near the limit of the near wake region ($x/R=6$), in the transition region and in the far wake ($x/R=10$ and 15). In each figure, the upper sub-plots refer to the case with laminar inflow and the lower sub-plots refer to the case with turbulent inflow. It can be seen that, for both laminar and turbulent inflow cases, the streamwise velocity increases with the blockage ratio. Note that the velocity reduction through the rotor is mitigated while the velocity increase outside of the rotor is enhanced due to the blockage effect [21]; hence the wake becomes slightly narrower but the difference between the maximum and minimum velocities does not change significantly as the blockage ratio increases (at least up to $\beta=0.2$ studied here). This explains, at least partly, why the blockage ratio does not affect the wake mixing rate significantly.

Similarly, normalized Reynolds stresses $\frac{\bar{u}'\bar{v}'}{k}$ are compared in Fig. 9 for different turbulence and blockage conditions. Again the effect of blockage is not clearly seen in this figure. However, of interest is the change of profiles at different streamwise locations. In the far wake, the values of the normalized Reynolds stresses across the wake edges are about -0.3 (around $y/R=1$) and 0.3 (around $y/R=-1$), showing that the far wake is similar to that of a bluff body. At the vicinity of the rotor ($x/R=0.5$), however, the direction (or sign) of the Reynolds stresses across the wake edges is opposite to that in the far wake, indicating that these stresses act in such a way as to increase (rather than decrease) the mean streamwise velocity difference between inside and outside the wake (presumably due to the effect of tip vortices).

4.2. Blockage effects on the blade loadings

Next we examine the effects of blockage and tip speed ratio on the computed local angle of attack α and the local velocities on the blades as they determine the blade loadings. Figs. 10 and 11 compare the calculated local angle of attack and velocities along the blade for the case of laminar free stream at three tip speed ratios of $\lambda=1$ (red), $\lambda=6$ (black), and $\lambda=12$ (blue). The first

¹ NTU is defined as the time required for a particle, traveling at the mean inflow velocity, to pass the entire computational domain.

² Throughout this paper, velocities are normalized by the free stream bulk velocity U_0 , stress components as well as TKE are normalized by U_0^2 , and blade loadings are normalized by $\rho U_0^2 R$.

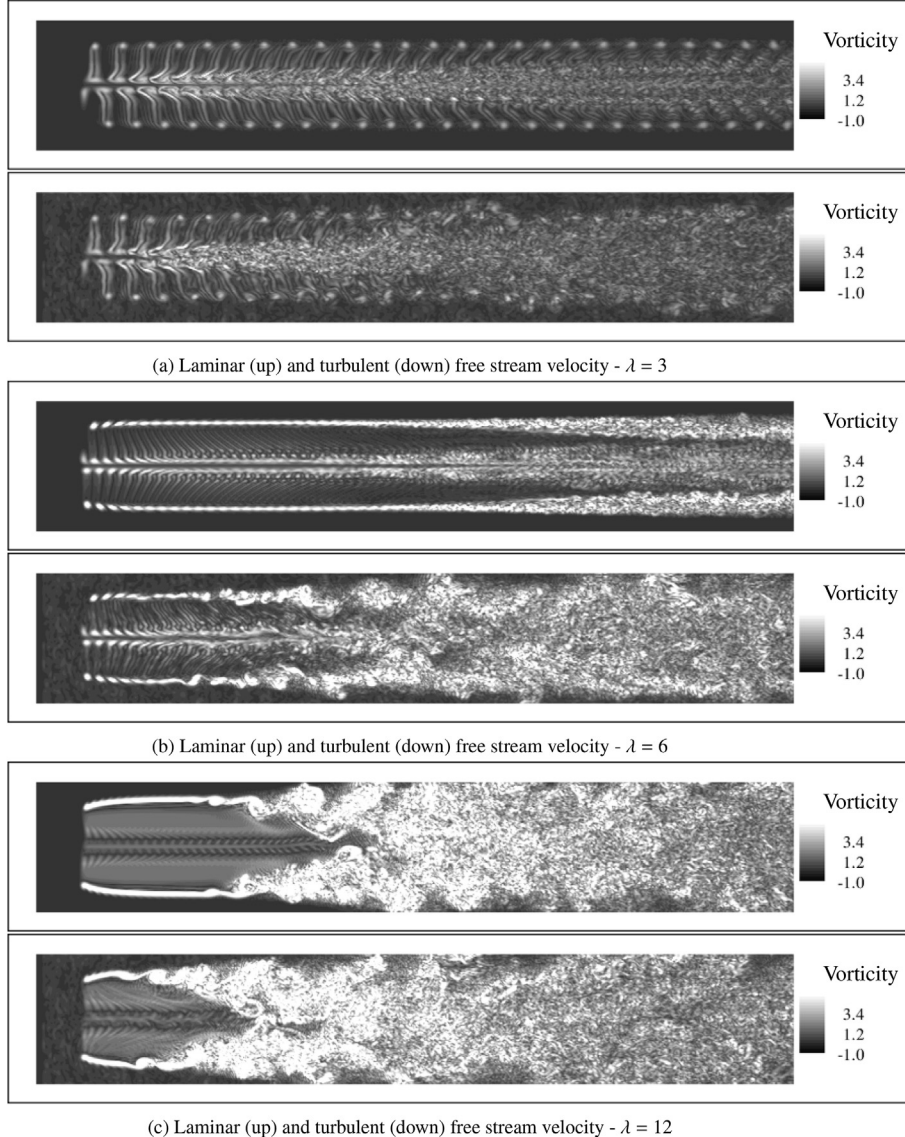


Fig. 15. Vorticity contours at different tip speed ratios for a blockage ratio of $\beta=0.20$.

observation is that the effect of blockage is insignificant on the local angles of attack. Among other phenomena, it can be clearly identified how the local angle of attack decreases with increasing λ .

The effects of blockage and tip speed ratio on the tangential and normal forces per unit blade length, normalized by the square of inlet velocity, are plotted in Fig. 12. Interestingly, the tangential force becomes heavily influenced by the blockage with increasing λ , while no such effects can be recognized for the case at $\lambda=1$. Looking at the normal forces, the blockage effects are less significant. It can also be seen from the blue lines in both figures that the tangential loading becomes negative at the inboard part of the rotor (around $x/R \leq 0.4$), indicating that the inner part of the rotor at the off-design condition ($\lambda=12$) operates in a propeller state.

4.3. Blockage effects on the optimal tip speed ratio

Figs. 13 and 14 illustrate the effects of blockage ratio on the power and thrust coefficients, respectively. Several cases were considered for the laminar free stream with tip speed ratios of 1, 3, 4, 5, 6, 7, 8, 10, and 12. In addition, computations were performed

for the turbulent free stream with tip speed ratios of 3, 6, and 12 to cover the whole range of operational conditions. Shown on top of the plots in blue star markers are experimental measurements, for which the blockage ratio is about 0.1 [10]. From the measurements, it can be noticed that the turbine operates in a heavily loaded condition when the tip speed ratio is above 8 (corresponding to thrust coefficients above 1). Also, at tip speed ratios smaller than 4, the effect of blockage ratio on both thrust and power coefficients are negligible. However, with increase in λ , the blockage effect becomes apparent with the power and thrust coefficients for the $\beta=0.2$ case becoming significantly greater than the other cases. It can also be inferred from the results that the optimal tip speed ratio (to maximize the power coefficient) slightly increases with the blockage ratio. These results agree qualitatively with recent RANS BEM simulations of a turbine in a channel [36] and confirm that any blockage ratio greater than 0.1 will impact the turbine performance substantially.

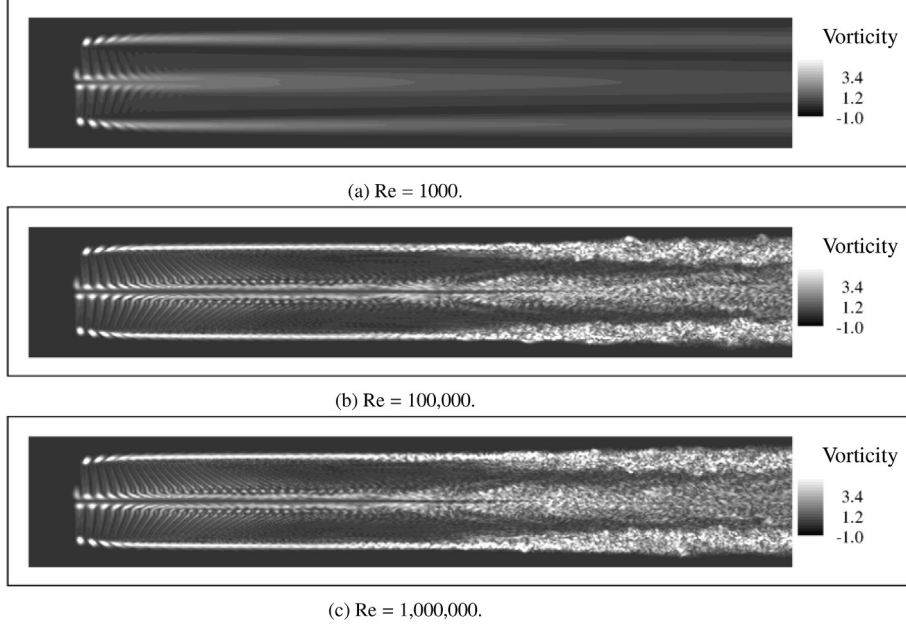


Fig. 16. Effect of Reynolds number of the vorticity contours in laminar inflow with $\lambda = 6$ for $\beta=0.09$.

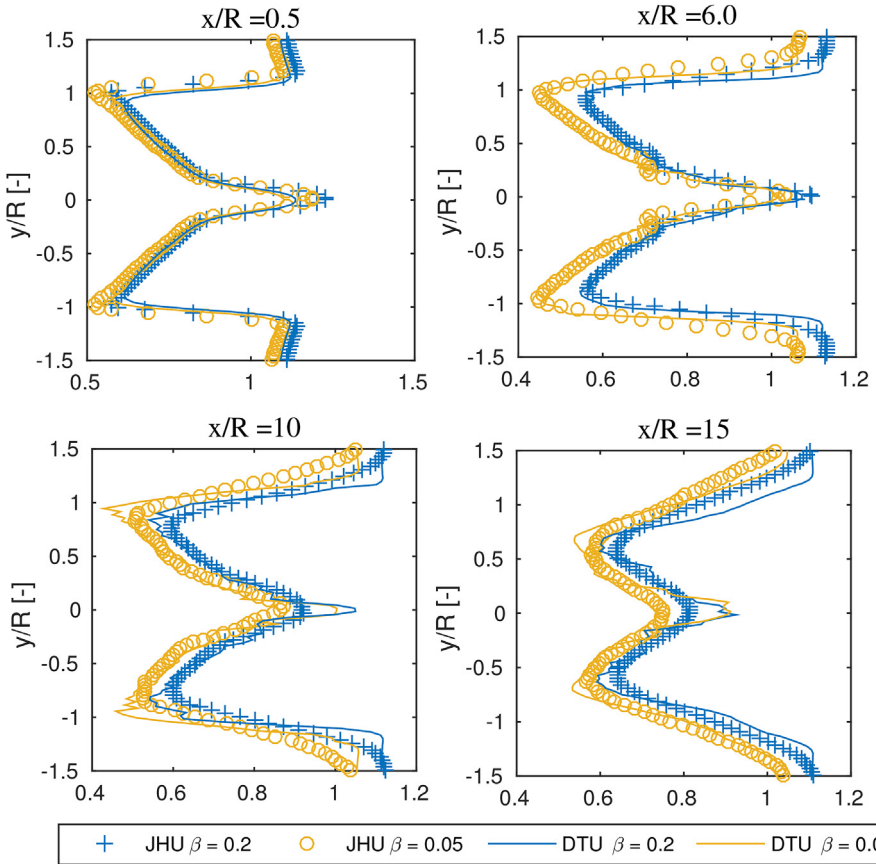


Fig. 17. Comparison of the mean velocity profiles between DTU and JHU codes for the laminar free stream flow at $\lambda = 6$ using $\beta=0.2$ and $\beta=0.05$.

4.4. Effects of the tip speed ratio and free stream turbulence

Fig. 15 shows vorticity contours obtained for the case $\beta=0.2$ (smallest test section) in laminar and turbulent free stream

conditions. As can be observed, in both laminar and turbulent free stream cases, a general trend is that the tip speed ratio has an inverse relationship with the streamwise location of the vortex pairing and break-down. Attention should also be paid to the fact

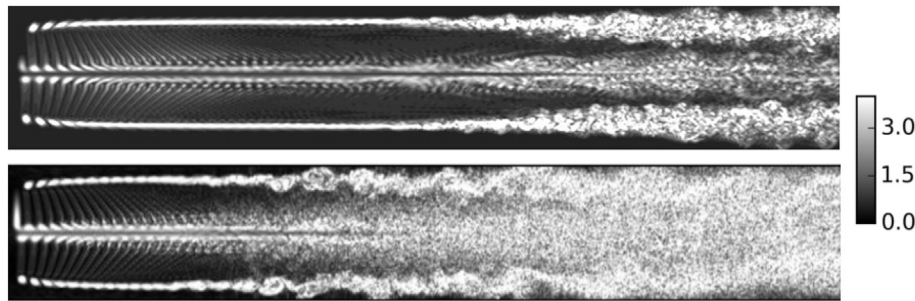


Fig. 18. Comparison of vorticity contours obtained using DTU (top) and JHU (bottom) codes in laminar free stream with $\lambda = 6$ and $\beta=0.05$.

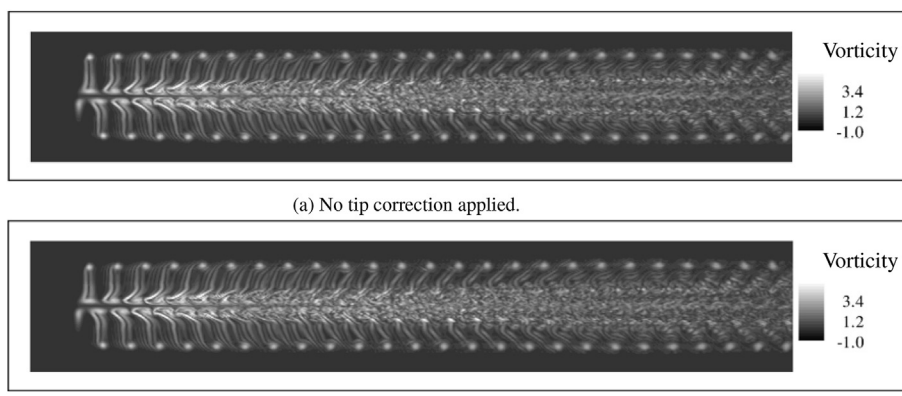


Fig. 19. Vorticity contours in laminar inflow at $\lambda = 3$ for $\beta=0.2$.

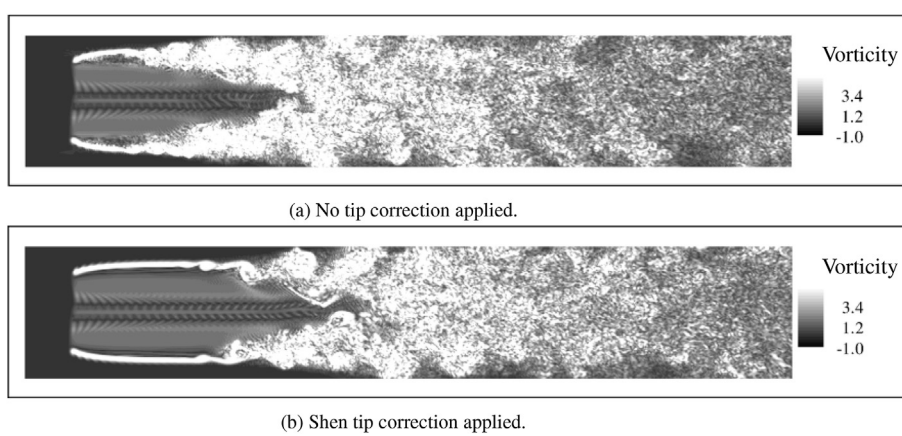


Fig. 20. Vorticity contours in laminar inflow at $\lambda = 12$ for $\beta=0.2$.

that especially at low values of λ , the free stream turbulence has a strong effect on breaking up the tip vortices. For instance, while the tip vortices are clearly visible in Fig. 15-a (up) for the laminar inflow, the pairing and break down of tip vortices occur at less than 3 rotor diameters downstream of the rotor plane in the turbulent free stream counterpart, as shown in Fig. 15-a (down).

4.5. Effect of Reynolds number

While most of the simulations are performed at the Reynolds number (based on rotor radius) of $Re = 100,000$, two cases at $Re = 1000$ and $Re = 1,000,000$ have also been performed in order to quantify the effect of Reynolds number on the development of

vortical structures downstream of the rotor. Fig. 16 shows the comparisons. As can be appreciated, at $Re = 1000$ breakdown of tip vortices is prevented and the wake remains laminar. Conversely, for the two highest Reynolds numbers, there are no visible differences, consistent with converged asymptotic behavior at high-Reynolds number.

4.6. Effect of LES code selection

The effects of using different numerical methods and subgrid scale models are studied for the two distinct blockage cases of $\beta=0.2$ and $\beta=0.05$. Only the cases with laminar inflow and $\lambda=6$ are presented. Other tip speed ratios were also considered and the

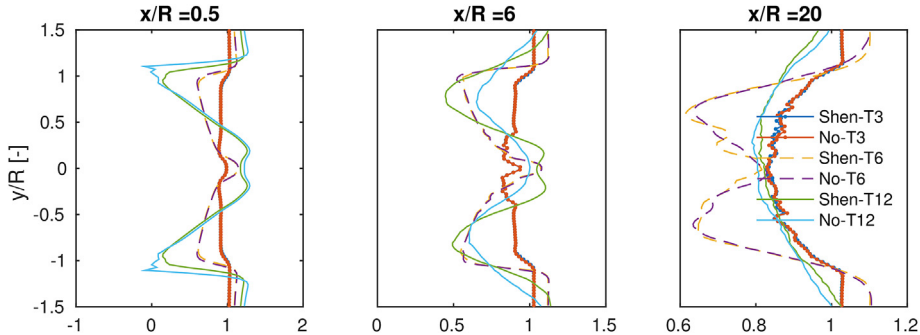


Fig. 21. Visualization of tip correction effects on the mean velocity profiles for the case with $\beta=0.2$ at laminar inflow. Shen-T3: Shen tip correction with tip speed ratio of 3; No-T3: No tip correction with tip speed ratio of 3, and similarly for $\lambda=6$ and $\lambda=12$.

comparisons led to similar conclusions. Results comparing mean velocity profiles are shown in Fig. 17 and comparisons of instantaneous vorticity distributions are presented in Fig. 18. As can be seen in the mean velocity profiles at $x/R=0.5$ and $x/R=6$, there is excellent agreement among the results obtained from the two codes. The only minor differences can be observed at $x/R=0.5$ near the tip region of the blades, where the discrepancies can be ascribed to the fact that the JHU code did not employ a tip correction (for more details on effects of tip correction, see the next subsection). At $x/R=6$ this effect has washed out and the two codes predict very similar mean velocity profiles. Further downstream at $x/R=10$ there still is good agreement among the results from the two codes. At $x/R=15$ one begins to see some differences due to the fact that for the pseudospectral code the wake has transitioned earlier and the presence of increased turbulence has smeared the mean velocity profile significantly. Overall, there is good agreement between the two codes' predictions of confinement effects on the wake.

4.7. A note on the effect of tip correction

Since the introduction by Ref. [25], models for tip loss correction (correction of circulation in the momentum equations to account for finite number of blades) have been an essential part of the blade element momentum theory [6,37,38]. In principle, no tip correction is required for the actuator line model, as it already takes into account the finiteness of the blades. However, as the loadings are distributed along lines representing each blade, the impact of the chord-wise load distribution is neglected. As discussed in a recent paper by Refs. [41,42], this effect modifies the airfoil data in the proximity of the tip. Hence a correction of the airfoil data or the loading is required to ensure that the loading tends gradually to zero near the tip of the blade. In the present work this effect is approximately taken into account by the empirical correction model introduced by Refs. [37,38] for actuator line methods.

It should be mentioned that due to lack of resolved experimental data (to date), no detailed conclusions can be drawn from the applicability of tip correction models when an actuator line is used. Nevertheless, it is insightful to compare the results for the two approaches. Comparisons are made at the extreme cases, that is, $\lambda=3$ and 12 at the smallest tunnel test sections corresponding to $\beta=0.2$. Figs. 19 and 20 show the comparisons at the low and high tip speed ratios, respectively. As can be realized from the figures, the effects of tip loss corrections are more significant at high tip speed ratios.

In order to quantitatively investigate the tip correction effects, the mean streamwise velocities obtained from the laminar free stream simulations at the smallest domain ($\beta=0.2$) are compared

at the three different tip speed ratios and plotted in Fig. 21. As can be seen, near the rotor and near the tip, the mean velocity profiles show significant differences.

5. Conclusions

In this paper, we studied the effects of wind tunnel blockage on the characteristics of wind turbine wakes as well as turbine performance. Other factors such as tip speed ratio, free stream turbulence, and Reynolds number were also investigated. We have demonstrated that LES provides a robust tool to study important physical effects such as blockage effects on the wake characteristics of a wind turbine; the results of LES can therefore be useful for a better understanding of wind tunnel experiments and comparisons with simulations. It should be noted that purely potential flow analysis is not sufficient to build up confidence since the wake growth depends on details of turbulence in the wake. For the same reason, RANS simulations are not very suitable either especially in predicting the details of flow structures such as helical tip vortices and their breakdown. LES results have shown that the blockage effect tends to increase with the tip speed ratio of the turbine. When the tip speed ratio is much lower than the optimal value, the blockage effect is insignificant on both power and thrust coefficients as well as on the wake characteristics (at least for the blockage ratio of up to 0.2 studied here). When the tip speed ratio is close to or above the optimal value, however, blockage ratios of larger than 0.05 will affect both tangential and normal forces on the blades and thus on the power and thrust coefficients. At the highest blockage ratio of 0.2, the mean velocity of the wake is also affected significantly, although no significant effects of the blockage on the wake mixing rate were observed in this study.

Finally, the comparison between two entirely different LES codes has indicated that the results obtained in this study are reasonably robust with respect to numerical methods, grid resolution, and subgrid-scale models used in the simulations.

Acknowledgments

HS and JNS acknowledge financial support from the Danish Council for Strategic Research for the project 'Center for Computational Wind Turbine Aerodynamics and Atmospheric Turbulence', COMWIND (grant 2014-09-067216/DSF) and for the support from the European Union's Seventh Program for Research, Technological Development and Demonstration for the project 'AdVanced Aerodynamic Tools for lArge Rotors', AVATAR (FP7-ENERGY-2013-1/no. 608396). LAMT was supported by NSF (IGERT), while international travel and CM were supported by NSF (IAA 124382, the WINDINSPIRE project).

References

- [1] B. Akay, C.S. Ferreira, G. van Bussel, G. Tescione, Experimental and numerical investigation of the effect of rotor blockage on wake expansion, in: Proceedings of the Conference on the Science of Making Torque from Wind, 2010, pp. 1–6.
- [2] M. Allan, A Cfd Investigation of Wind Tunnel Interference on Delta Wing Aerodynamics, Ph.D. thesis, University of Glasgow, 2002.
- [3] E. Bou-Zeid, C. Meneveau, M. Parlange, A scale-dependent lagrangian dynamic model for large eddy simulation of complex turbulent flows, *Phys. Fluids* 17 (2) (2005) 025105.
- [4] M. Calaf, C. Meneveau, J. Meyers, Large eddy simulation study of fully developed wind-turbine array boundary layers, *Phys. Fluids* 22 (1) (2010) 015110.
- [5] T. Chen, L. Liou, Blockage corrections in wind tunnel tests of small horizontal-axis wind turbines, *Exp. Therm. Fluid Sci.* 35 (3) (2011) 565–569.
- [6] H. Glauert, Airplane propellers, in: *Aerodynamic Theory*, Springer, 1935, pp. 169–360.
- [7] R.I. Issa, Solution of the implicitly discretised fluid flow equations by operator-splitting, *J. Comput. Phys.* 62 (1) (1986) 40–65.
- [8] R.-j. Jiang, J.-z. Lin, Wall effects on flows past two tandem cylinders of different diameters, *J. Hydrom. Ser. B* 24 (1) (2012) 1–10.
- [9] A. Jimenez, A. Crespo, E. Migoya, J. Garcia, Advances in large-eddy simulation of a wind turbine wake, *J. Phys. Conf. Ser.* 75 (1) (2007) 012041.
- [10] P.-Å. Krogstad, P. Eriksen, Blind test calculations of the performance and wake development for a model wind turbine, *Renew. Energy* 50 (2013) 325–333.
- [11] J. Mann, Wind field simulation, *Probab. Eng. Mech.* 13 (4) (1998) 269–282.
- [12] L. Martinez-Tossas, M. Churchfield, C. Meneveau, Large eddy simulation of wind turbine wakes: detailed comparisons of two codes focusing on effects of numerics and subgrid modeling, *J. Phys. Conf. Ser.* 625 (2015) 012024.
- [13] S. McTavish, D. Feszyt, F. Nitzsche, An experimental and computational assessment of blockage effects on wind turbine wake development, *Wind Energy* 17 (10) (2014) 1515–1529.
- [14] D. Medici, S. Ivanell, J.-Å. Dahlberg, P.H. Alfredsson, The upstream flow of a wind turbine: blockage effect, *Wind Energy* 14 (5) (2011) 691–697.
- [15] C. Meneveau, J. Katz, Scale-invariance and turbulence models for large-eddy simulation, *Annu. Rev. Fluid Mech.* 32 (1) (2000) 1–32.
- [16] R. Mikkelsen, Actuator Disc Methods Applied to Wind Turbines, Ph.D. thesis, Technical University of Denmark, 2003.
- [17] R. Mikkelsen, J. Sørensen, S. Øye, N. Troldborg, Analysis of power enhancement for a row of wind turbines using the actuator line technique, *J. Phys. Conf. Ser.* 75 (2007) 012044.
- [18] M. Mokry, Y. Chan, D. Jones, Two-dimensional Wind Tunnel Wall Interference, 1983. Tech. rep., No. AGARD-AG-281.
- [19] K. Nilsson, S. Ivanell, K.S. Hansen, R. Mikkelsen, J.N. Sørensen, S.-P. Breton, D. Henningson, Large-eddy simulations of the lillgrund wind farm, *Wind Energy* 18 (3) (2015) 449–467.
- [20] T. Nishino, S. Draper, Local blockage effect for wind turbines, *J. Phys. Conf. Ser.* 625 (2015) 012010.
- [21] T. Nishino, R.H.J. Willden, Effects of 3-d channel blockage and turbulent wake mixing on the limit of power extraction by tidal turbines, *Int. J. Heat Fluid Flow* 37 (2012) 123–135.
- [22] S. Patankar, *Numerical Heat Transfer and Fluid Flow*, CRC Press, 1980.
- [23] P. Patil, S. Tiwari, Effect of blockage ratio on wake transition for flow past square cylinder, *Fluid Dyn. Res.* 40 (11) (2008) 753–778.
- [24] U. Piomelli, Wall-layer models for large-eddy simulations, *Prog. Aerosp. Sci.* 44 (6) (2008) 437–446.
- [25] L. Prandtl, A. Betz, *Vier Abhandlungen zur Hydrodynamik und Aerodynamik...: mit einer Literaturübersicht als Anhang*, Kaiser Wilhelm-Instituts für Strömungsforschung, 1927.
- [26] C. Rhee, W. Chow, Numerical study of the turbulent flow past an airfoil with trailing edge separation, *AIAA J.* 21 (11) (1983) 1525–1532.
- [27] J. Ryi, W. Rhee, U.C. Hwang, J.-S. Choi, Blockage effect correction for a scaled wind turbine rotor by using wind tunnel test data, *Renew. Energy* 79 (2015) 227–235.
- [28] P. Sagaut, *Large Eddy Simulation for Incompressible Flows*, vol. 3, Springer, Berlin, 2000.
- [29] H. Sarlak, *Large Eddy Simulation of Turbulent Flows in Wind Energy*, Ph.D. thesis, Technical University of Denmark, 2014.
- [30] H. Sarlak, C. Meneveau, J. Sørensen, Role of subgrid-scale modelling in large eddy simulation of wind turbine wake interactions, *Renew. Energy* 77 (2015) 386–399.
- [31] H. Sarlak, C. Meneveau, J. Sørensen, R. Mikkelsen, Quantifying the impact of subgrid scale models in actuator-line based les of wind turbine wakes in laminar and turbulent inflow, in: *Direct and Large-eddy Simulation IX*, Springer, 2015, pp. 169–175.
- [32] H. Sarlak, F. Pierella, R. Mikkelsen, J. Sørensen, Comparison of two les codes in wind turbine wake interactions, *J. Phys. Conf. Ser.* 524 (1) (2014) 012145.
- [33] H. Sarlak, J. Sørensen, Large eddy simulation of wind turbine wakes in prescribed neutral and non-neutral atmospheric boundary layers, *J. Phys. Conf. Ser.* 555 (2014) 012087.
- [34] H. Sarlak, J. Sørensen, R. Mikkelsen, Large eddy simulation of atmospheric boundary layer over wind farms using a prescribed boundary layer approach, *AIP Conf. Proc.* 121 (2012) 121–124.
- [35] S. Sarmast, H. Sarlak, S. Ivanell, R. Mikkelsen, Numerical investigation of the wake interaction between two model wind turbines with spanwise offset, *J. Phys. Conf. Ser.* 524 (1) (2014) 012137.
- [36] J. Schluntz, R. Willden, The effect of blockage on tidal turbine rotor design and performance, *Renew. Energy* 81 (2015) 432–441.
- [37] W.Z. Shen, R. Mikkelsen, J.N. Sørensen, C. Bak, Tip loss corrections for wind turbine computations, *Wind Energy* 8 (4) (2005) 457–475.
- [38] W.Z. Shen, J.N. Sørensen, R. Mikkelsen, Tip loss correction for actuator/navier-stokes computations, *J. Sol. Energy Eng.* 127 (2) (2005) 209–213.
- [39] J. Sørensen, W. Shen, Numerical modeling of wind turbine wakes, *J. Fluids Eng.* 124 (2) (2002) 393.
- [40] J.N. Sørensen, Instability of helical tip vortices in rotor wakes, *J. Fluid Mech.* 682 (2011) 1–4.
- [41] J.N. Sørensen, K.O. Dag, N. Ramos-García, A refined tip correction based on decambering, *Wind Energy* (2015), <http://dx.doi.org/10.1002/we.1865>. Article first published online: 15 May 2015.
- [42] J.N. Sørensen, R.F. Mikkelsen, D.S. Henningson, S. Ivanell, S. Sarmast, S.J. Andersen, Simulation of wind turbine wakes using the actuator line technique, *Philos. Trans. Royal Soc. Lond. Math. Phys. Eng. Sci.* 373 (2035) (2015) 20140071.
- [43] J.N. Sørensen, W.Z. Shen, R. Mikkelsen, Wall correction model for wind tunnels with open test section, *AIAA J.* 44 (8) (2006) 1890–1894.
- [44] L. Ta Phuoc, Modèles de sous-maille appliqués aux écoulements instationnaires et décollés, *Journée Thématique DRET*, Paris, 1994.
- [45] N. Troldborg, J. Sørensen, R. Mikkelsen, Actuator line simulation of wake of wind turbine operating in turbulent inflow, *J. Phys. Conf. Ser.* 75 (1) (2007) 012063.